

## Contents lists available at ScienceDirect

# Vacuum

journal homepage: www.elsevier.com/locate/vacuum



## Short communication

# Robust method for surface modulation in Cu-Zn alloys via pulsed laser surface melting

Justin Hijam<sup>a</sup>, Alok Kumar<sup>a</sup>, Madhu Vadali<sup>a</sup>, Pradipta Ghosh<sup>b</sup>, Raghavan Ranganathan<sup>b,\*</sup>

- <sup>a</sup> Department of Mechanical Engineering, Indian Institute of Technology Gandhinagar, Gujarat, 382355, India
- <sup>b</sup> Department of Materials Engineering, Indian Institute of Technology Gandhinagar, Gujarat, 382355, India

#### ARTICLE INFO

Handling Editor: Luigia Sabbatini

Keywords:
Pulsed laser surface melting
Segregation
Cu-Zn brass
Molecular dynamics simulations

#### ABSTRACT

This study investigates the segregation behaviour of Zn in Cu-Zn brass during pulsed laser surface melting (pLSM), through a combination of experiments and molecular dynamics (MD) simulations. Understanding the segregation phenomena is critical for tailoring surface properties in alloys, which has significant implications for improving material performance in demanding applications. Starting from a  $Cu_{90}Zn_{10}$  random solid solution brass alloy, well-defined, Zn-rich annular regions that contain about 35 % Zn arise due to segregation during pLSM and subsequent solidification. MD simulations reveal that Zn atoms possess significantly higher mobility than Cu during both the melting and solidification stages, leading to pronounced surface segregation, corroborating experiments. This selective surface enrichment of Zn holds promise for enhancing corrosion resistance and surface hardness in brass alloys, paving way for further optimization of alloy compositions and laser processing parameters to achieve tailored surface properties in brasses and other alloy systems.

## 1. Introduction

Laser surface melting (LSM) is an advanced technique employed in material processing to modify surface properties and enhance the performance of various materials [1]. Pulsed LSM (pLSM) is a subcategory where ultra-fast high intensity laser pulses are employed to rapidly heat and melt the surface of a material, leading to significant changes in its surface topography [2,3], microstructure [4] and properties [5–7]. The high pulsed laser energy melts a thin layer of a localised area, developing a melt pool. The flow within the melt pool induced by surface tension forces leads to redistribution of the molten layer which, upon solidification, leads to newer surface features [8]. The precise control over the laser parameters allows for tailored modifications, making pLSM a valuable tool in manufacturing processes where surface characteristics are critical.

Due to the high energy and process of solidification involved, alloy segregation during this process is a phenomenon of significant interest as it can substantially impact the material's properties. Researchers have employed high temperature processing of alloys to induce chemical segregation to improve the properties of the material [9]. Shyam et al. [10] showed that the segregation of Mn and Zr at specific interfaces in a Al-Cu alloy assisted in improving the mechanical properties. Similar

trends of segregation were also observed in laser-based additive manufacturing [11–13]; however, this phenomenon is yet to be explored for pLSM to the best of our knowledge. This segregation can lead to the formation of regions with varying compositions, which in turn have the capability to enhance mechanical properties, corrosion resistance, and overall performance. Understanding the mechanisms driving this segregation is essential for optimizing pLSM processes and achieving the desired material properties.

Molecular dynamics (MD) simulations have emerged as a powerful tool for studying segregation phenomena in alloys. For instance, investigations using MD on binary metal nanoparticles, such as Ni-Cu and Au-Ag, revealed the segregation of Cu and Ag, respectively [14]. Similarly, MD studies on surface segregation in liquid semiconductor Si-Ge alloys showed the segregation of Ge [15]. Moreover, many researchers have employed MD in laser-based manufacturing processes to gain insights into topics such as grain growth, crack repair, and defect formation during the process [16,17]. The level of atomistic detail provided by MD is particularly valuable for understanding the effects of rapid heating and cooling during pLSM, which are challenging to capture through experimental techniques alone. MD studies thus offer a complementary perspective to experimental analyses, facilitating a comprehensive understanding of alloy behaviour during laser processing.

E-mail address: rraghav@iitgn.ac.in (R. Ranganathan).

<sup>\*</sup> Corresponding author.

This study investigates segregation in Cu-Zn brass during pLSM using experiments and MD simulations. The brass composition used is  $10\,\%$  Zn and 90 % Cu. By integrating these approaches, the aim is to provide a detailed investigation of the mobility and distribution of Cu and Zn atoms during the melting and solidification processes.

#### 2. Experimental and computational methods

The pLSM experiments were carried out using a 300 W, 1080 nm fiber laser (SPI Lasers, redPOWER QUBE, model SP-0300-C-A-020–05-PQA-011–001-000). The laser beam was delivered to a 2D scan head (hurrySCAN 20) with a 255 mm f-theta objective lens, producing a near-Gaussian beam ( $M^2=1.1$ ) with a  $1/e^2$  radius of 19.8  $\mu$ m at the focal plane. The processing chamber consists of a manual stage with accessible z-direction movement allowing adjustment of the beam size. Fig. 1 (a) shows a schematic of the laser setup. All processing was performed in open air, as using an argon atmosphere at high energy densities led to nanoparticle deposition. However, selected experiments were also conducted under argon and varying energy densities to study the influence of atmosphere and temperature on segregation. Elemental distribution of Cu and Zn was analysed using EDS (JEOL JSM-7900F SEM), while phase analysis was done via XRD (BRUKER D8 DISCOVER).

All MD simulations in this study were conducted using the open-source parallel simulator LAMMPS (Large-Scale Atomic/Molecular Massively Parallel Simulator) [18]. OVITO, an open-source software package, was utilised for geometry visualisation and post-processing analysis [19]. The current simulation investigates the mobility of Cu and Zn atoms during pLSM of brass.

MD simulations were first employed to estimate the melting point of bulk brass. A cubic simulation box (36.84 Å per side) containing 4000 atoms with 10 % Zn randomly distributed was used, with periodic boundary conditions applied in all directions to mimic bulk behaviour. The system was relaxed under the NPT ensemble at 300 K for 1 ns, followed by heating from 300 K to 2000 K over another 1 ns. A sharp change in potential energy and density around 1420 K indicates the onset of melting. This predicted melting temperature is  $\sim$ 18 % higher than the experimental value ( $\sim$ 1200 K), which is consistent with known MD trends. The overprediction arises from the use of periodic boundaries and the absence of nucleation sites under constant heating rates [20,21], and thus still validates the interatomic potential used. The

latent heat of melting obtained from the simulation is  $\sim$ 128 kJ/kg, reasonably close to the reported value of 153.2 kJ/kg [22].

Fig. 1(b-d) shows the initial configuration for the MD simulations. The computational box consists of three regions: the melt pool region (region  $\Omega$ ), the bulk region (region  $\Pi$ ) and the vacuum region (region  $\Sigma$ ). The melt pool is hemispherical with a diameter of 147.36 Å, representing localised heating by a Gaussian laser source during pLSM. The entire simulation box is of the size of 368.4 Å X 221 Å X 221 Å. A vacuum region  $\Sigma$  is present till a height of 36.84 Å which is followed by atomfilled region of  $\Omega \cup \Pi$  of height 147.4 Å. The atom-filled region is topped by another vacuum region  $\sum$  of height 184.2 Å. A total number of 583200 atoms are present in region  $\Omega \cup \Pi$  out of which 10 % of atoms are defined to be Zn. The initial lattice of Cu-Zn brass alloy is created to be a disordered Face Centred Cubic lattice, where the positions of 10 % of the atoms are randomly assigned to be of type Zn. This composition is commensurate with the calculated composition from Energy-dispersive X-ray spectroscopy (EDS) analysis. Periodic boundary conditions are applied along x and y directions, while reflective walls are applied in the z direction at location of z=36.84 Å and z=190 Å. The reflective wall binds the atoms to the designated region and reflects the atoms (a small fraction of them) back in the region when they attempt to cross the wall.

The initial configuration is relaxed to reach equilibrium by allowing the simulation box to relax under the NPT ensemble at 300 K for 1 ns, with reflective walls in the z direction inactive during this stage. After the initial relaxation at 300 K, the next steps for the MD simulation are melting and solidification. During the melting process, the region  $\Omega$  is heated from the temperature of 300 K-2000 K at a linear rate for 1 ns with 0.1 bar pressure using the NVT ensemble. The upper bound temperature is 2000 K, well above the bulk melting point, to ensure complete melting. For region  $\Pi$ , the atoms are integrated with NVT ensemble to maintain the temperature of 300 K for 1 ns. Between the melting and solidification phases, a second equilibrium phase is maintained such that region  $\Omega$  and region  $\Pi$  are held at 2000 K and 300 K, respectively, for 1 ns using the NVT ensemble. For the solidification stage, the temperature of region  $\Omega$  is reduced from 2000 K to 300 K linearly over 10 ns using the NVT ensemble, while region  $\Pi$  is kept at 300 K using the NVT ensemble for 10 ns. The Nose-Hoover thermostat and barostat were used for the NVT and NPT equilibration stages as included in LAMMPS. For the current metallic system, the Embedded Atom Method (EAM) potentials

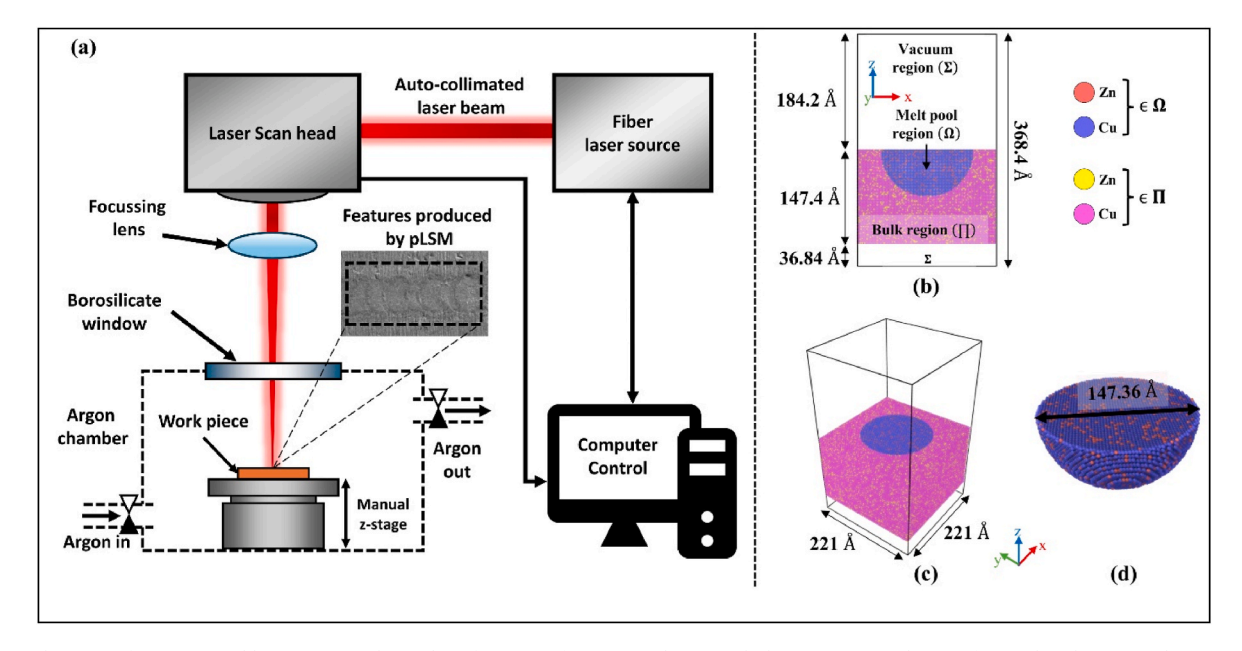


Fig. 1. (a) Schematic of experimental laser set up and initial configuration for MD simulation with (b) cross-sectional view of atom distribution, and isometric view of atom distribution for (c) all regions, and (d) melt pool region.

for Cu-Zn were used which are fully parameterised based on *ab-initio* simulations [23]. It is important to note the large difference in length scale of the experiment and simulation because of the limitation of the computational resources. However, the scaled-down simulation was still able to shed light on the mechanism of alloy segregation during LSM.

#### 3. Results and discussion

During pLSM and subsequent solidification, Zn atoms were observed to segregate and cluster at the surface. EDS analysis of the pLSMed brass sample confirms Zn migration and clustering at the top surface, as shown in Fig. 2(a). These features, with a diameter of  $\sim$ 92  $\mu$ m, were produced using laser power of 210 W and 5000  $\mu$ s pulse duration, resulting in a surface Zn concentration of  $\sim$ 35 %. Furthermore, XRD analysis (Fig. 2(b)) reveals that the bare brass sample exhibits only Cu-Zn solid solution peaks, while the pLSMed sample shows additional ZnO

peaks, indicating surface oxidation during open-air processing. These peaks align with patterns reported for heated brass by Zhou et al. [24]. The formation of ZnO during open-air pLSM is not only indicative of surface oxidation but also plays a critical role in enhancing corrosion resistance. ZnO acts as a stable and adherent barrier layer that restricts the ingress of oxygen and moisture, thereby suppressing electrochemical activity and mitigating dezincification in brass alloys [25]. Although direct corrosion testing was not performed in this study, prior literature has demonstrated that even low ZnO content significantly improves corrosion resistance [26,27]. Additionally, comparative experiments conducted under open air and argon atmospheres confirmed consistent Zn surface enrichment in both environments, suggesting that Zn segregation is robust across processing conditions.

Experiments under open air and argon atmospheres at a reduced pulse duration of 500  $\mu$ s showed comparable Zn segregation (~20 %) on the surface (Fig. 2(c)). It was also observed that pulse durations

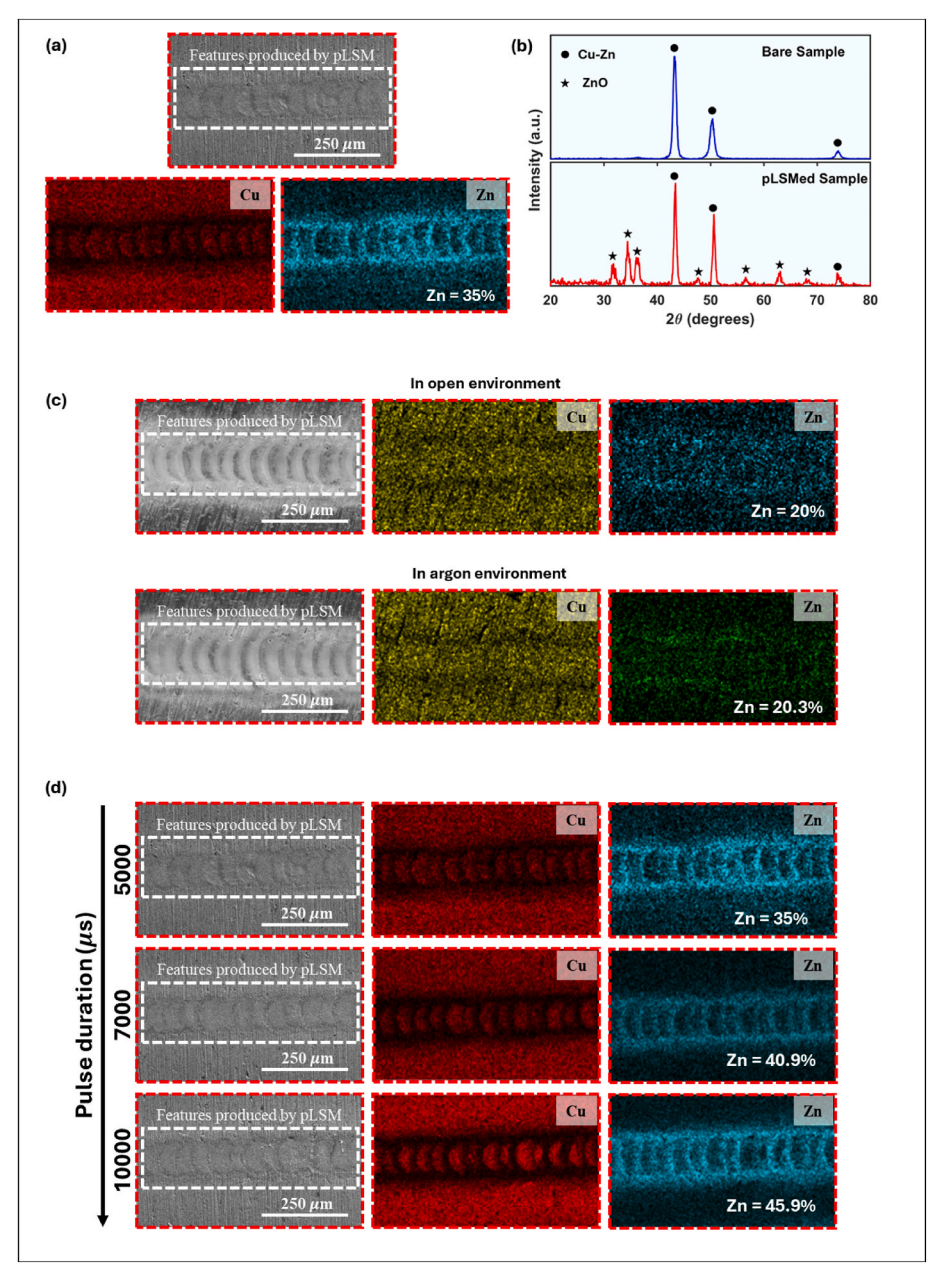


Fig. 2. (a) EDS analysis showing the clustering of Zn atoms at the top surface after pLSM, (b) X-ray diffraction patterns for bare and pLSMed samples, (c) EDS analysis showing the clustering of Zn atoms at the top surface after pLSM in open and controlled environment and (d) EDS analysis showing the clustering of Zn atoms at the top surface after pLSM with different pulse durations.

exceeding 500 µ s in argon environment, due to higher energy densities, commonly result in nanoparticle deposition on the surface which is a known phenomenon in high-energy-density laser material processing [28,29]. To determine the optimal laser parameters for achieving Zn surface segregation while avoiding nanoparticle deposition, a systematic approach was adopted. Starting from lower energy densities, the pulse duration was gradually increased while maintaining a fixed power of 210 W. Complete surface melting and formation of defined laser spots were first observed at a pulse duration of 500  $\mu$ s, which was taken as the baseline. Subsequent experiments at longer durations (5000–10000  $\mu$ s) revealed progressively enhanced Zn segregation, with the most consistent ring-like pattern emerging at 5000 µs. Notably, nanoparticle deposition was observed only in the argon environment beyond 500 µs, attributed to vapour plume condensation, whereas open-air conditions vielded clean surfaces even at higher energy densities. These observations guided the selection of 210 W and >5000 µs as the optimal parameters for inducing Zn surface enrichment without surface contamination. This stepwise methodology is consistent with approaches reported in prior work for identifying melting and ablation regimes in pLSM [2]. A direct relationship between input energy density and Zn segregation was also observed. Increasing the pulse duration from 5000 µs to 7000 µs led to a progressive rise in surface Zn concentration to ~35 %, 41 %, and 46 %, respectively (Fig. 2(d)), highlighting the potential to tailor surface composition by tuning laser parameters.

The bare (unprocessed) sample is crystalline, and this crystallinity is retained even after solidification following pLSM. Similar recrystallisation upon cooling has been reported in laser-treated materials [30-32]. Both the bare and pLSMed samples exhibit a crystalline but disordered solid solution, a feature also captured in the MD simulations. Fig. 3(a-b) shows the post-solidification lattice structure of the region  $\Omega$ . Initially, 88.8 % of atoms are arranged in the FCC lattice, with atoms at the top surface and around the periphery of region  $\Omega$  deviating from the FCC packing. Upon heating beyond the melting point, the region transitions to liquid, however, after solidification, 63 % of the atoms revert to FCC packing. During the melting and solidification process, many atoms diffuse to the surface, where they do not follow the FCC structure. Nonetheless, the MD simulations successfully capture the atoms regaining their crystalline structure, as observed in the experimental XRD findings. It should be noted that for simplicity, oxidation effects during the pLSM process are not modelled in this study. Furthermore, Fig. 3(c-d) shows the Zn and Cu distribution before and after solidification.

A significant fraction of Zn atoms migrates to the surface during

pLSM. Quantitative analysis of the MD results was performed to evaluate the composition within a 10 Å depth from the top surface in region  $\Omega$ . In the initial configuration, Zn atoms made up  $\sim$ 10 % of this region, which increased to  $\sim$ 35 % after solidification.

To further investigate Zn redistribution, the simulation box along the z-direction was divided into 0.5 Å bins, and the number of Zn atoms per bin within region  $\Omega$  was calculated (Fig. 4(a)). Initially, Zn atoms were confined below 184.2 Å. However, post-solidification, a significant number of Zn atoms appeared above this height, forming a distinct surface layer. This is evident from the large number of Zn atoms present beyond the height of 184.2 Å in the post-solidification configuration, corroborating our experimental results (Fig. 2(a)). Moreover, increasing the input energy density led to wider melt pools and a higher degree of Zn segregation to the surface. This trend highlights the potential for tuning surface composition and properties through precise control of pLSM parameters.

The mean squared displacement (MSD) for Zn and Cu atoms in region  $\Omega$  during heating and solidification is shown in Fig. 4(b–c). During both the melting and the solidification stages, Zn atoms exhibit higher MSD than Cu in all directions, indicating enhanced diffusivity. Notably, higher MSD of Zn in the z direction highlights their greater vertical mobility, enabling surface migration.

To characterise the segregation of Zn along the lateral dimensions (x and y axes), Fig. 4(d–e) compares the distribution of the Zn atoms along the x and y axes belonging originally to the region  $\Omega$ , but located at heights of z  $\geq$  180 Å. The distribution of Zn at initial and post-solidification remains symmetric along x and y, reflecting the axisymmetric nature of pLSM. However, a clear increase in Zn count is observed post-solidification, attributed to the upward migration of interior Zn atoms that then spread laterally at the surface. Interestingly, Zn atoms tend to accumulate more at the periphery than at the centre of region  $\Omega$  in both directions. This ring-like distribution matches experimental results, where Zn clustering is observed around the edges of laser-processed features (See Fig. 2(a)).

Fig. 5 shows the evolution of Zn concentration within two regions of the melt pool during molecular dynamics (MD) simulations: Region 1 (z  $\geq$  180 Å), representing the surface, and Region 2 (134 Å  $\leq$  z  $\leq$  144 Å), representing the interior, as illustrated in Fig. 5 (a). The Zn distribution is analysed across three distinct phases: (I) melting, (II) relaxation at 2000 K, and (III) solidification. From Fig. 5(b), it is evident that Zn segregation at the surface (Region 1) progressively increases through all three phases, with the most pronounced enrichment occurring during solidification. The corresponding average

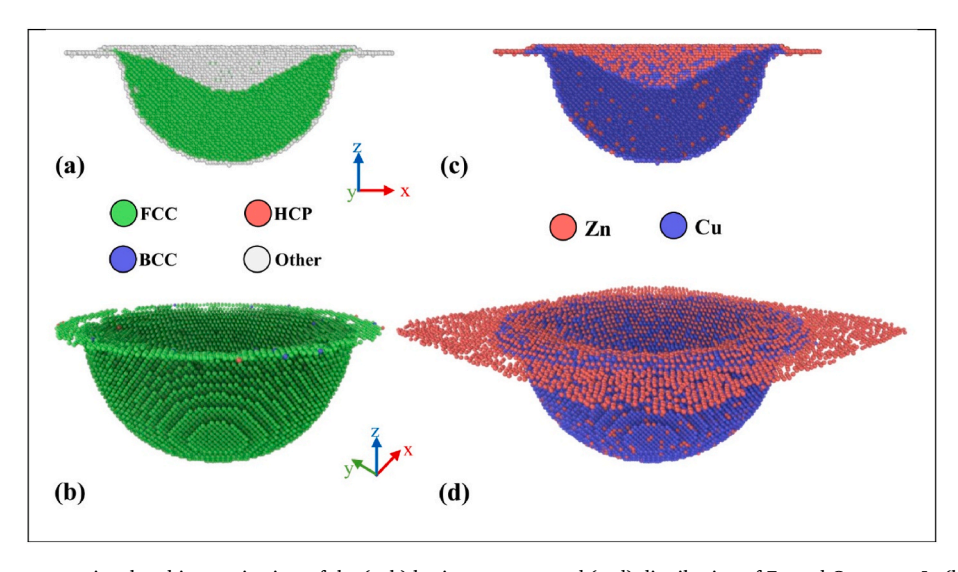
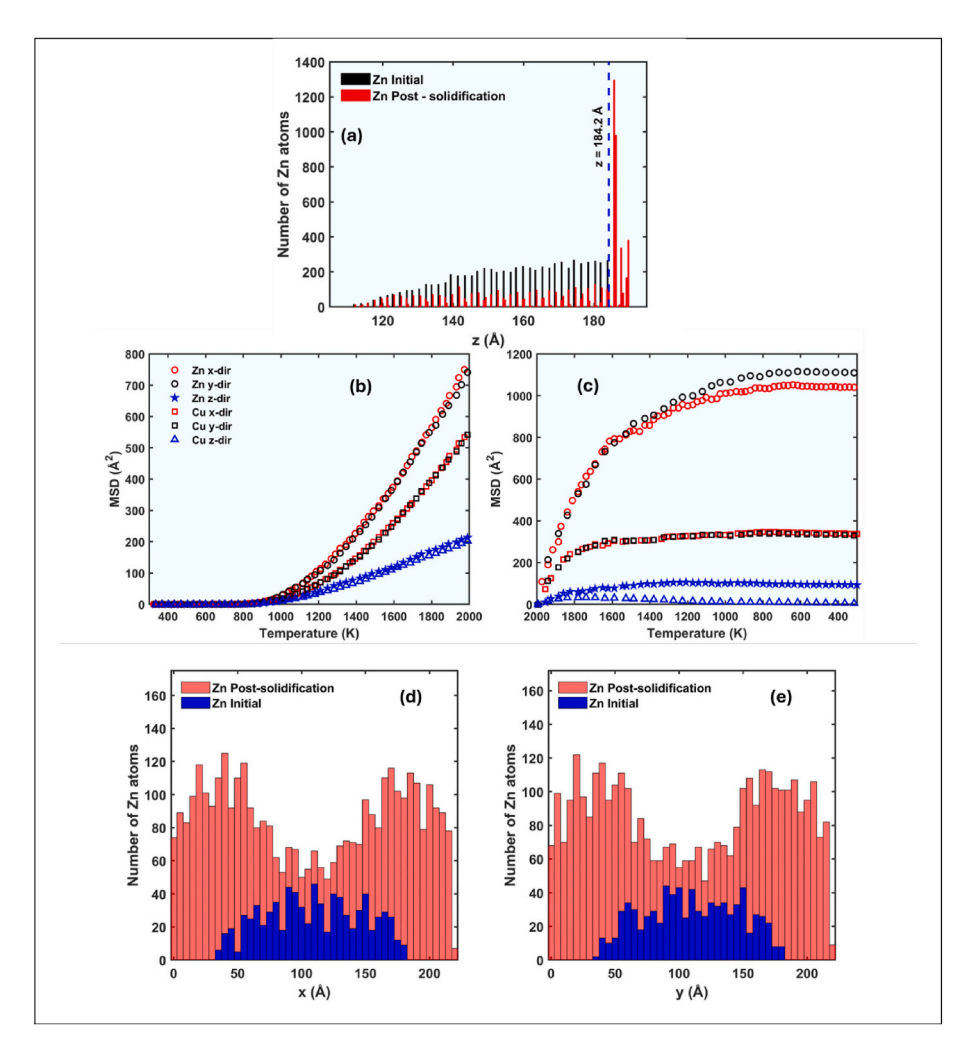


Fig. 3. Post-solidification cross-sectional and isometric view of the (a–b) lattice structure and (c–d) distribution of Zn and Cu atoms. In (b), the atoms belonging to the 'other' category are removed for better visualisation.



**Fig. 4.** (a) Number of Zn atoms at different z height bins at initial and after-solidification configuration and (b–c) Mean squared displacement (MSD) calculated for Zn and Cu atoms along the x, y and z directions for atoms in the region  $\Omega$  during (b) melting and (c) solidification stages and comparison of the distribution of Zn atoms in post-solidification and initial configuration along the (d) x and the (be) y axes.

temperature of all atoms within the  $\Omega$  domain is also plotted for reference.

It is important to note that the spatial and temporal scales accessible through MD simulations are inherently smaller than those encountered in experiments. To ensure the mechanistic validity of the simulation outcomes, a systematic scaling analysis was conducted. Three simulations were performed to examine the sensitivity of Zn segregation behaviour to both time and system size. In Simulation 2 (Fig. 5(c)), the heating, relaxation, and solidification durations were each extended by a factor of three compared to the baseline case of Simulation 1 (Fig. 5 (b)). In Simulation 3 (Fig. 5(e)), the original time scales were retained, but the simulation box size and number of atoms were reduced to half. In all three cases, the Zn surface enrichment behaviour remained consistent, with the Zn concentration at the surface stabilising around  $\sim$ 35 %. These consistent outcomes, despite variations in simulation time and size, confirm that Zn segregation is not an artifact of accelerated MD dynamics or limited domain size, but instead reflects intrinsic physical drivers such as higher diffusivity and vapour pressure of Zn relative to Cu. The agreement with experimentally observed Zn enrichment further supports the scale-independent mechanistic reliability of the MD results in representing Zn migration during pulsed laser surface melting.

It is known that Zn exhibits significantly higher vapour pressures than Cu at a given temperature, indicating a greater tendency to enter the vapour phase [33]. As Cu reaches its solidification point at 1357 K, Zn still has a high vapour pressure, suggesting that Zn atoms retain

significant mobility at this temperature. This difference in vapour pressure implies that Zn atoms are more likely to migrate to the surface compared to Cu atoms in the same environment. This characteristic can play a crucial role during solidification processes, where Zn's higher vapour pressure supports its continued redistribution and migration, even under conditions where Cu has already solidified.

While the present study did not include thermal or mechanical stability testing of the Zn-rich surface layers, the potential risk of interdiffusion at elevated temperatures is acknowledged. However, this risk is considered manageable for many practical applications, particularly due to the presence of a ZnO surface layer, which can serve as a diffusion barrier. Prior studies have shown that ZnO exhibits high thermal stability and low diffusivity, thereby limiting atomic exchange and enhancing surface durability [34–37]. Furthermore, the shallow nature of the segregated Zn layer produced by pLSM inherently reduces the likelihood of deep interdiffusion-driven degradation. These considerations, while not experimentally explored in the current work, are important for long-term application and form the basis for future work focused on thermal cycling, wear resistance, and interdiffusion profiling.

#### 4. Conclusions

In summary, the current study integrates MD simulations and experimental analyses, to provide a comprehensive demonstration of Zn atom migration and surface clustering during pLSM of brass, phenomena

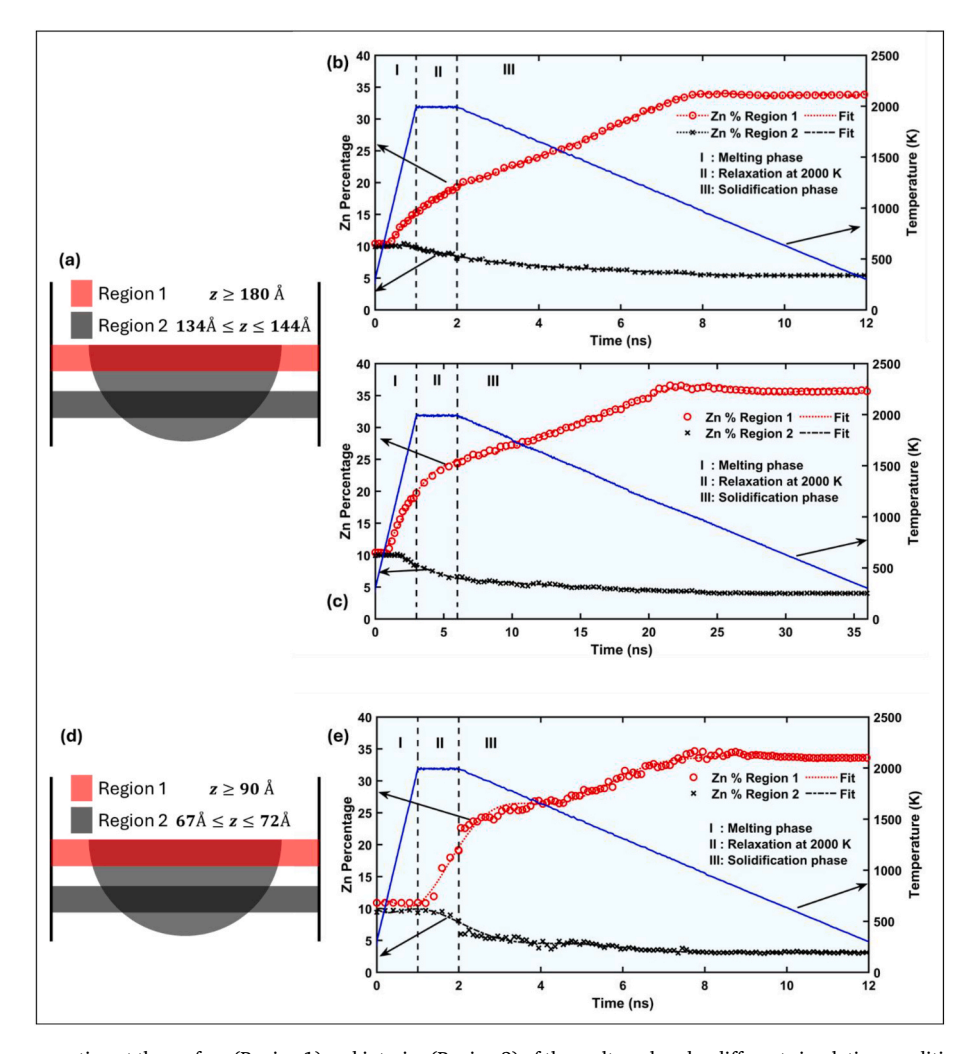


Fig. 5. Comparison of Zn segregation at the surface (Region 1) and interior (Region 2) of the melt pool under different simulation conditions. (a) and (d) illustrate the spatial binning used to define the surface and interior regions. (b) and (c) show the temporal evolution of Zn percentage in both regions for total simulation durations of 12 ns and 36 ns, respectively. (e) presents the Zn distribution for a 12 ns simulation in which both the system size and the number of atoms were halved.

that can be important for tailoring the material properties of alloys. The results reveal that Zn atoms exhibit significantly higher mobility than Cu atoms during both the melting and solidification stages, leading to a pronounced and robust segregation of Zn at the surface. Understanding the Zn atom segregation during pLSM allows for the precise control of surface composition, which can be harnessed to enhance specific properties of brass alloys. For instance, the increased presence of Zn at the surface can improve corrosion resistance [38,39] and surface hardness [40,41], making these materials more suitable for demanding applications in various industries. We believe that there is immense scope in optimization of pLSM parameters for tailoring segregation in alloy systems that have reasonable solid solubility along with significantly different elemental mobility or partial vapour pressure in the liquid phase for engineering customized surface properties.

#### CRediT authorship contribution statement

Justin Hijam: Writing – original draft, Visualization, Validation, Software, Methodology, Investigation, Formal analysis, Data curation, Conceptualization. Alok Kumar: Methodology, Investigation, Formal analysis, Data curation. Madhu Vadali: Writing – review & editing, Supervision, Resources, Project administration, Methodology, Conceptualization. Pradipta Ghosh: Writing – review & editing, Validation, Resources, Methodology, Investigation. Raghavan Ranganathan: Writing – review & editing, Supervision, Project administration,

 $Methodology, \, Investigation, \, Formal \, analysis, \, Conceptualization.$ 

## Declaration of competing interest

The authors declare that they have no known competing financial interests or personal relationships that could have appeared to influence the work reported in this paper.

## Acknowledgements

The authors acknowledge IIT Gandhinagar's Param Ananta supercomputing facility for all the simulations reported in this work. This research did not receive any specific grant from funding agencies in the public, commercial, or not-for-profit sectors.

#### Data availability

Data will be made available on request.

#### References

- J. Hijam, R. Balhara, M. Vadali, Investigating double-scan strategies for reducing heat-affected zone in laser surface melting, Opt Laser. Technol. 170 (2024) 110289, https://doi.org/10.1016/j.optlastec.2023.110289.
- [2] R. Gupta, J. Hijam, R. Balhara, M. Vadali, Design of Micro-scale Periodic Surface Textures by Pulsed Laser Melting and its Influence on Wettability. Volume 2:

- Manufacturing Processes; Manufacturing Systems, American Society of Mechanical Engineers, West Lafayette, Indiana, USA, 2022, https://doi.org/10.1115/MSEC2022-85829. V002T05A058.
- [3] A. Sassmannshausen, A. Brenner, J. Finger, Ultrashort pulse laser polishing by continuous surface melting, J. Mater. Process. Technol. 293 (2021) 117058, https://doi.org/10.1016/j.jmatprotec.2021.117058.
- [4] J. Zhang, M. Yu, Z. Li, Y. Liu, Q. Zhang, R. Jiang, et al., The effect of laser energy density on the microstructure, residual stress and phase composition of H13 steel treated by laser surface melting, J. Alloys Compd. 856 (2021) 158168, https://doi. org/10.1016/j.jallcom.2020.158168.
- [5] Hashemi S. Hamid, S. Ali Mousavi, R. Shoja Razavi, A. Nourollahi, A. Ashrafi, Laser surface melting of al–co–rare earth (Ce–La) alloys for improving corrosion resistance, Opt Laser. Technol. 162 (2023) 109256, https://doi.org/10.1016/j. optlastec.2023.109256.
- [6] R. Liu, J. Yu, Q. Yang, J. Wu, S. Gao, Mechanical property and strengthening mechanism on DH36 marine steel after laser surface melting, Surf. Coating. Technol. 425 (2021) 127733, https://doi.org/10.1016/j.surfcoat.2021.127733
- [7] K. Karami, A. Blok, L. Weber, S.M. Ahmadi, R. Petrov, K. Nikolic, et al., Continuous and pulsed selective laser melting of Ti6Al4V lattice structures: effect of postprocessing on microstructural anisotropy and fatigue behaviour, Addit. Manuf. 36 (2020) 101433, https://doi.org/10.1016/j.addma.2020.101433.
- [8] C. Ma, M. Vadali, N.A. Duffie, F.E. Pfefferkorn, X. Li, Melt pool flow and surface evolution during pulsed laser micro polishing of Ti6Al4V, J. Manuf. Sci. Eng. 135 (2013) 061023, https://doi.org/10.1115/1.4025819.
- [9] P.Y. Hou, Segregation phenomena at thermally grown Al 2 O 3/Alloy interfaces, Annu. Rev. Mater. Res. 38 (2008) 275–298, https://doi.org/10.1146/annurev. matsci.38.060407.130323.
- [10] A. Shyam, S. Roy, D. Shin, J.D. Poplawsky, L.F. Allard, Y. Yamamoto, et al., Elevated temperature microstructural stability in cast AlCuMnZr alloys through solute segregation, Mater. Sci. Eng., A 765 (2019) 138279, https://doi.org/ 10.1016/j.msea.2019.138279.
- [11] D. Karlsson, A. Marshal, F. Johansson, M. Schuisky, M. Sahlberg, J.M. Schneider, et al., Elemental segregation in an AlCoCrFeNi high-entropy alloy a comparison between selective laser melting and induction melting, J. Alloys Compd. 784 (2019) 195–203, https://doi.org/10.1016/j.jallcom.2018.12.267.
- [12] G. Luo, H. Xiao, S. Li, C. Wang, Q. Zhu, L. Song, Quasi-continuous-wave laser surface melting of aluminium alloy: precipitate morphology, solute segregation and corrosion resistance, Corros. Sci. 152 (2019) 109–119, https://doi.org/ 10.1016/j.corsci.2019.01.035.
- [13] S.A. Mantri, S. Dasari, A. Sharma, T. Alam, M.V. Pantawane, M. Pole, et al., Effect of micro-segregation of alloying elements on the precipitation behaviour in laser surface engineered alloy 718, Acta Mater. 210 (2021) 116844, https://doi.org/ 10.1016/j.actamat.2021.116844.
- [14] V.M. Samsonov, A.G. Bembel, AYu Kartoshkin, S.A. Vasilyev, I.V. Talyzin, Molecular dynamics and thermodynamic simulations of segregation phenomena in binary metal nanoparticles, J. Therm. Anal. Calorim. 133 (2018) 1207–1217, https://doi.org/10.1007/s10973-018-7245-4.
- [15] W. Yu, D. Stroud, Molecular-dynamics study of surface segregation in liquid semiconductor alloys, Phys. Rev. B 56 (1997) 12243–12249, https://doi.org/ 10.1103/PhysRevB.56.12243.
- [16] G. Singh, A.M. Waas, V. Sundararaghavan, Understanding defect structures in nanoscale metal additive manufacturing via molecular dynamics, Comput. Mater. Sci. 200 (2021) 110807, https://doi.org/10.1016/j.commatsci.2021.110807.
  [17] K. Peng, H. Huang, H. Xu, Y. Kong, L. Zhu, Z. Liu, A molecular dynamics study of
- [17] K. Peng, H. Huang, H. Xu, Y. Kong, L. Zhu, Z. Liu, A molecular dynamics study of laser melting of densely packed stainless steel powders, Int. J. Mech. Sci. 243 (2023) 108034, https://doi.org/10.1016/j.ijmecsci.2022.108034.
- [18] A.P. Thompson, H.M. Aktulga, R. Berger, D.S. Bolintineanu, W.M. Brown, P. S. Crozier, et al., LAMMPS a flexible simulation tool for particle-based materials modeling at the atomic, meso, and continuum scales, Comput. Phys. Commun. 271 (2022) 108171, https://doi.org/10.1016/j.cpc.2021.108171.
- [19] A. Stukowski, Visualization and analysis of atomistic simulation data with OVITO-the open visualization tool, Model. Simulat. Mater. Sci. Eng. 18 (2010) 015012, https://doi.org/10.1088/0965-0393/18/1/015012.
- [20] N. Joshi, N. Mathur, T. Mane, D. Sundaram, Size effect on melting temperatures of alumina nanocrystals: molecular dynamics simulations and thermodynamic modeling, Comput. Mater. Sci. 145 (2018) 140–153, https://doi.org/10.1016/j. commatsci.2017.12.064.
- [21] P.M. Agrawal, B.M. Rice, D.L. Thompson, Molecular dynamics study of the effects of voids and pressure in defect-nucleated melting simulations, J. Chem. Phys. 118 (2003) 9680–9688, https://doi.org/10.1063/1.1570815.

- [22] K. Härkki, J. Miettinen, Mathematical modeling of copper and brass upcasting, Metall. Mater. Trans. B 30 (1999) 75–98, https://doi.org/10.1007/s11663-999-000-6
- [23] A. Clement, T. Auger, An EAM potential for α-brass copper–zinc alloys: application to plasticity and fracture, Model. Simulat. Mater. Sci. Eng. 31 (2023) 015004, https://doi.org/10.1088/1361-651X/aca4ec.
- [24] L. Yuan, C. Wang, R. Cai, Y. Wang, G. Zhou, Spontaneous ZnO nanowire formation during oxidation of Cu-Zn alloy, J. Appl. Phys. 114 (2013) 023512, https://doi. org/10.1063/1.4812569.
- [25] L. Kenworthy, W.G. O'Driscoll, DEZINCIFICATION OF BRASSES. Anti-corrosion Methods and Materials, vol. 2, 1955, pp. 247–249, https://doi.org/10.1108/ eb019087
- [26] T.W. Quadri, L.O. Olasunkanmi, O.E. Fayemi, M.M. Solomon, E.E. Ebenso, Zinc oxide nanocomposites of selected polymers: synthesis, characterization, and corrosion inhibition studies on mild steel in HCl solution, ACS Omega 2 (2017) 8421–8437, https://doi.org/10.1021/acsomega.7b01385.
- [27] Samad U. Abdus, M.A. Alam, A. Anis, E.-S.M. Sherif, S.I. Al-Mayman, S.M. Al-Zahrani, Effect of incorporated ZnO nanoparticles on the corrosion performance of SiO2 nanoparticle-based mechanically robust epoxy coatings, Materials 13 (2020) 3767, https://doi.org/10.3390/ma13173767.
- [28] A. Mohanta, M. Leistner, M. Leparoux, Effect of plume dynamics on surface contamination during interaction of millisecond infrared fiber laser with titanium, Opt Laser. Eng. 153 (2022) 106996, https://doi.org/10.1016/j. optlaseng.2022.106996.
- [29] A. Mohanta, M. Leistner, M. Leparoux, Influence of temporal and spectral profiles of lasers on weld quality of titanium, Opt Laser. Eng. 134 (2020) 106173, https://doi.org/10.1016/j.optlaseng.2020.106173.
- [30] C.G. Woychik, D.H. Lowndes, T.B. Massalski, Solidification structures in melt-spun and pulsed laser-quenched Cu-Ti alloys, Acta Metall. 33 (1985) 1861–1871, https://doi.org/10.1016/0001-6160(85)90008-2.
- [31] M.V. Shugaev, M. He, Y. Levy, A. Mazzi, A. Miotello, N.M. Bulgakova, et al., Laser-induced thermal processes: heat transfer, generation of stresses, melting and solidification, vaporization, and phase explosion, in: K. Sugioka (Ed.), Handbook of Laser Micro- and Nano-Engineering, Springer International Publishing, Cham, 2021, pp. 83–163, https://doi.org/10.1007/978-3-030-63647-0\_11.
- [32] S.P. Zhvavyi, Simulation of the melting and crystallization processes in monocrystalline silicon exposed to nanosecond laser radiation, Tech. Phys. 45 (2000) 1014–1018, https://doi.org/10.1134/1.1307010.
- [33] G. Couturier, M. Rappaz, Effect of volatile elements on porosity formation in solidifying alloys, Model. Simulat. Mater. Sci. Eng. 14 (2006) 253–271, https://doi. org/10.1088/0965-0393/14/2/009.
- [34] A. Kołodziejczak-Radzimska, T. Jesionowski, Zinc oxide—from synthesis to application: a review, Materials 7 (2014) 2833–2881, https://doi.org/10.3390/ pag7042833
- [35] H.A. El-Wahab, E.K. Alenezy, N. Omer, M.A. Abdelaziz, R. Jame, S.A. Alshareef, et al., Efficacy of zinc and copper oxide nanoparticles as heat and corrosion-resistant pigments in paint formulations, Sci. Rep. 14 (2024), https://doi.org/10.1038/s41598-024-74345-0
- [36] E.A. Franco-Urquiza, J.F. May-Crespo, C.A. Escalante Velázquez, R. Pérez Mora, P. González García, Thermal degradation kinetics of ZnO/polyester nanocomposites, Polymers 12 (2020) 1753, https://doi.org/10.3390/ polym12081753.
- [37] F. Jones, H. Tran, D. Lindberg, L. Zhao, M. Hupa, Thermal stability of zinc compounds, Energy Fuels 27 (2013) 5663–5669, https://doi.org/10.1021/ ef400505u.
- [38] S. Anwar, F. Khan, Y. Zhang, S. Caines, Zn composite corrosion resistance coatings: what works and what does not work? J. Loss Prev. Process. Ind. 69 (2021) 104376 https://doi.org/10.1016/j.jlp.2020.104376.
- [39] J. Lim, G. Jeong, K. Seo, J. Lim, S. Park, W. Ju, et al., Controlled optimization of Mg and Zn in Al alloys for improved corrosion resistance via uniform corrosion, Mater. Adv. 3 (2022) 4813–4823. https://doi.org/10.1039/D1MA01220G.
- Adv. 3 (2022) 4813–4823, https://doi.org/10.1039/D1MA01220G.
  [40] K.C. Nnakwo, F.O. Osakwe, B.C. Ugwuanyi, P.A. Oghenekowho, I.U. Okeke, E. A. Maduka, Grain characteristics, electrical conductivity, and hardness of Zn-doped Cu–3Si alloys system, SN Appl. Sci. 3 (2021) 829, https://doi.org/10.1007/s42452-021-04784-1
- [41] E.M. Salleh, H. Zuhailawati, S. Ramakrishnan, M.A.-H. Gepreel, A statistical prediction of density and hardness of biodegradable mechanically alloyed Mg-Zn alloy using fractional factorial design, J. Alloys Compd. 644 (2015) 476–484, https://doi.org/10.1016/j.jallcom.2015.04.090.